A New Heterometallic Terbium(III)-Ruthenium(II) Complex and its Terbium(III)-Zinc(II) Analog: Syntheses, Characterization, Luminescence, and Electrochemical properties

A. John Maria Xavier, N. Arockia Samy, M. Wilson Bosco Paul, B. Brainard, M. Letticia, and V. Alexander*

Department of Chemistry, Loyola College, Chennai-600034, India.

Supporting Information

Figure S1. FAB mass spectrum of 2-(4-(2,2′:6′,2″)-terpyridin-4′-yl-benzyloxy)benzaldehyde (**L[1]**).

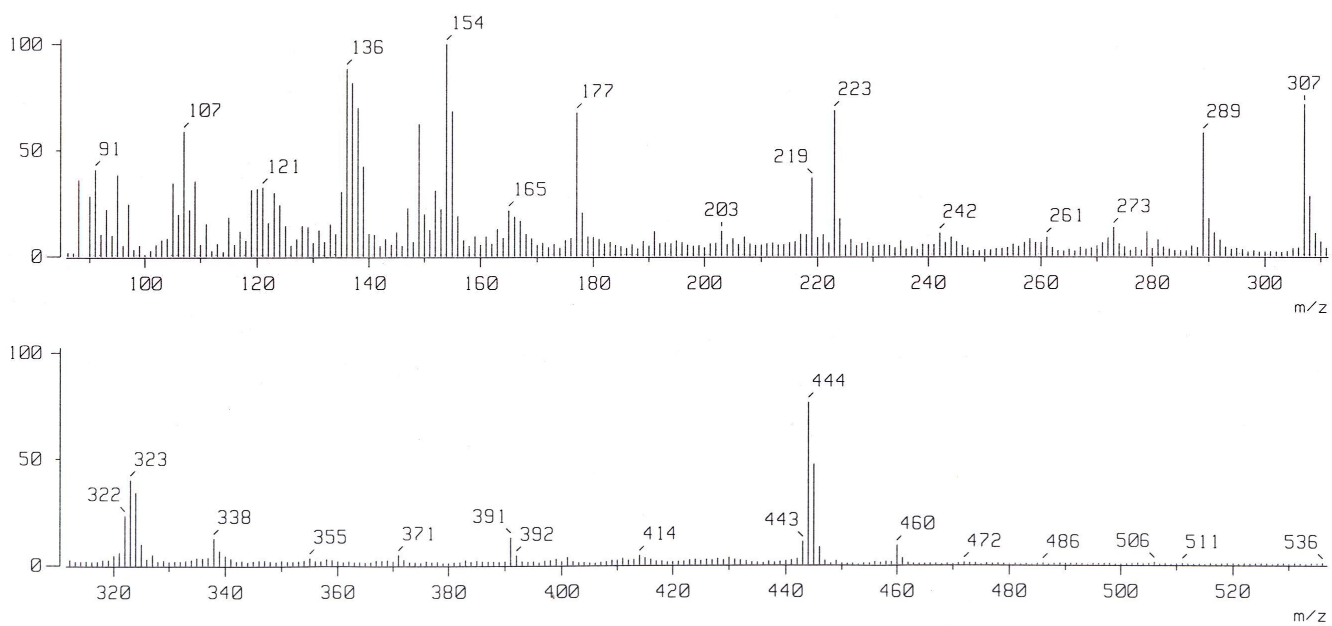

Figure S2. 500 MHz ^{1}H (*a*) and 125 MHz ^{13}C (*b*) NMR spectrum of 2-(4-(2,2′:6′,2″)-terpyridin-4′-yl-benzyloxy)benzaldehyde (**L¹**) in $CDCl_3$.

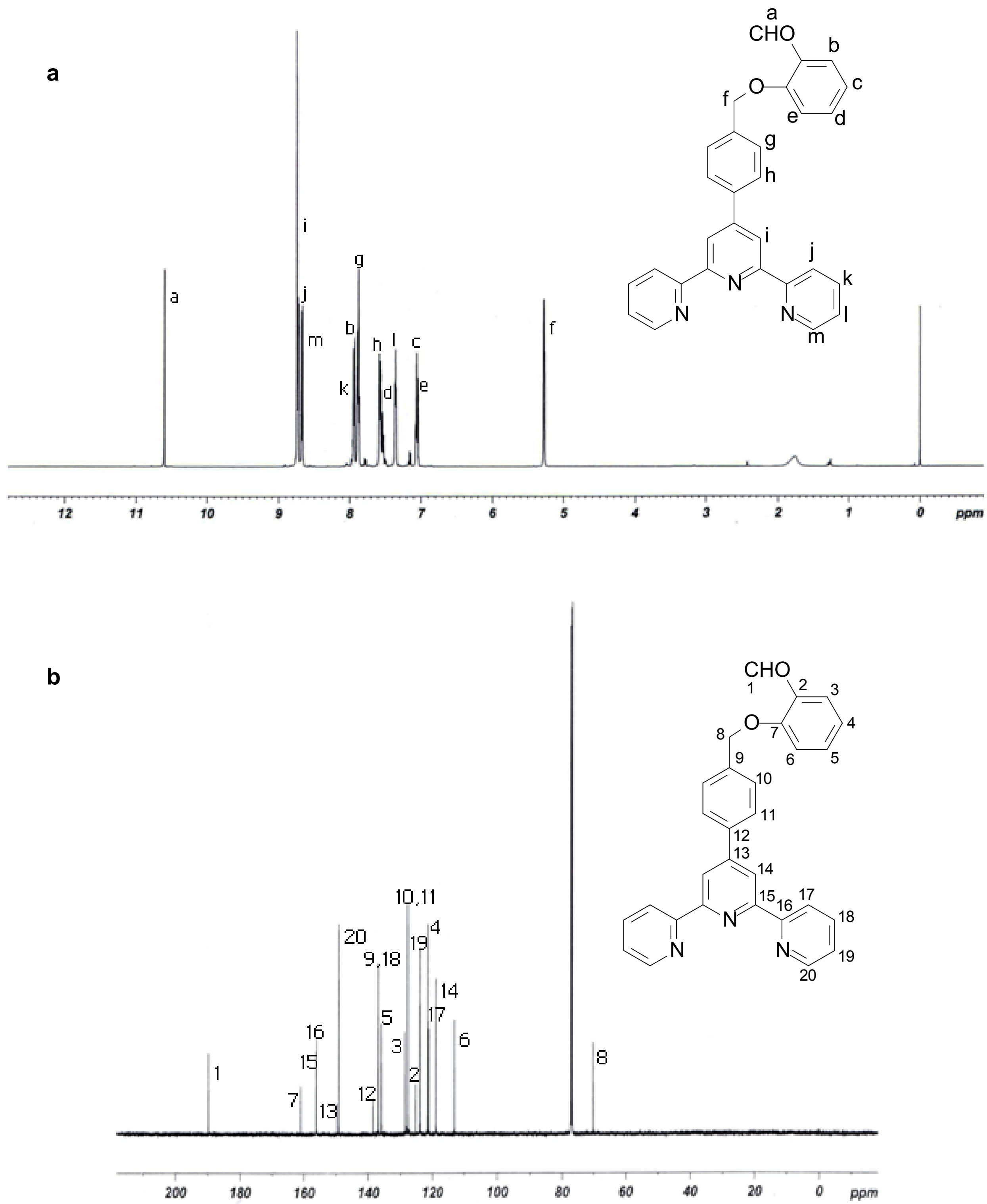

Figure S3. ESI mass spectrum of **L**[2].

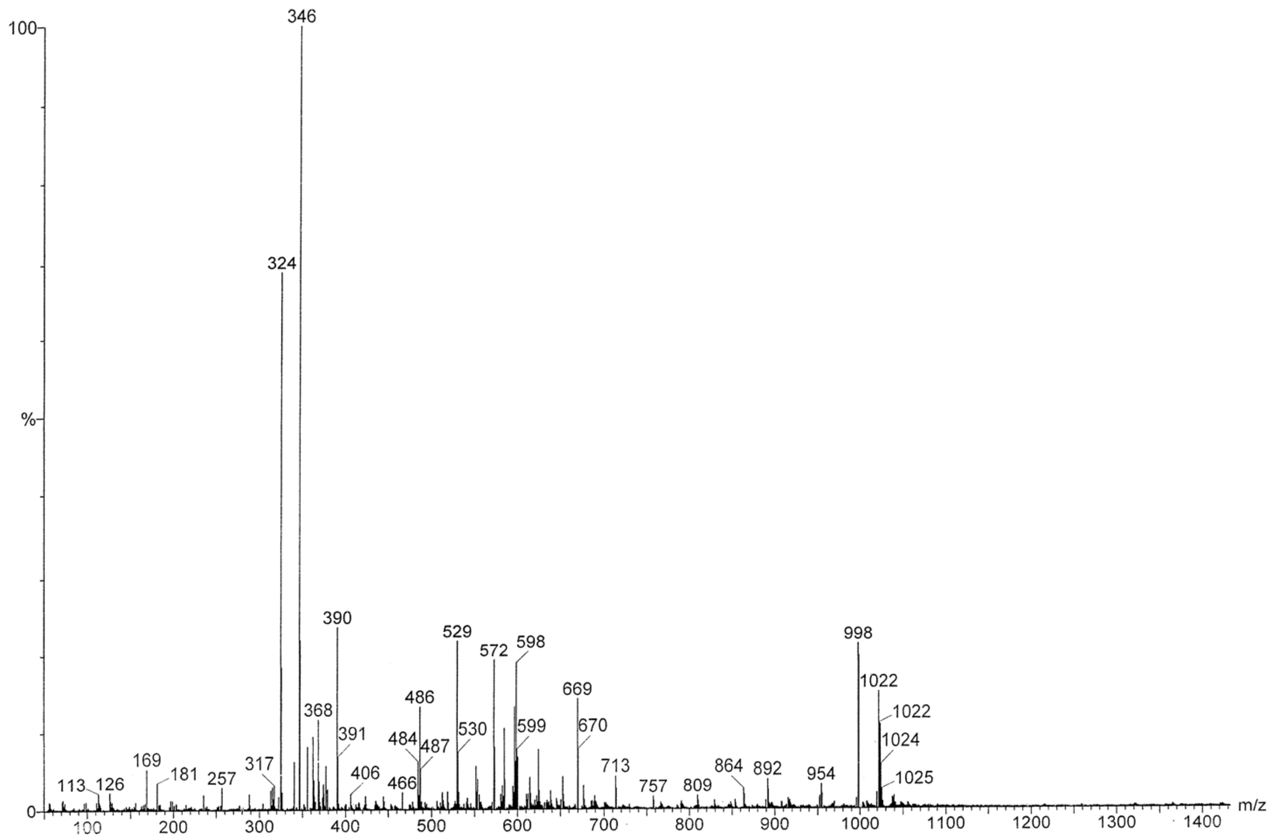

Figure S4. 500 MHz ^{1}H (*a*) and 125 MHz ^{13}C (*b*) NMR spectrum of $\mathbf{L^2}$ in $CDCl_3$.

a

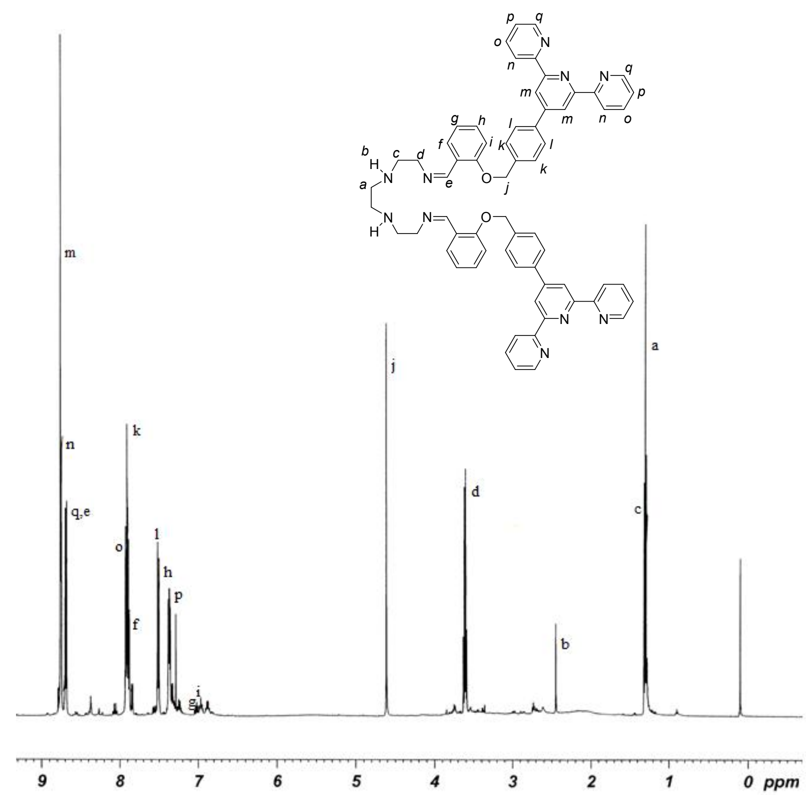

b

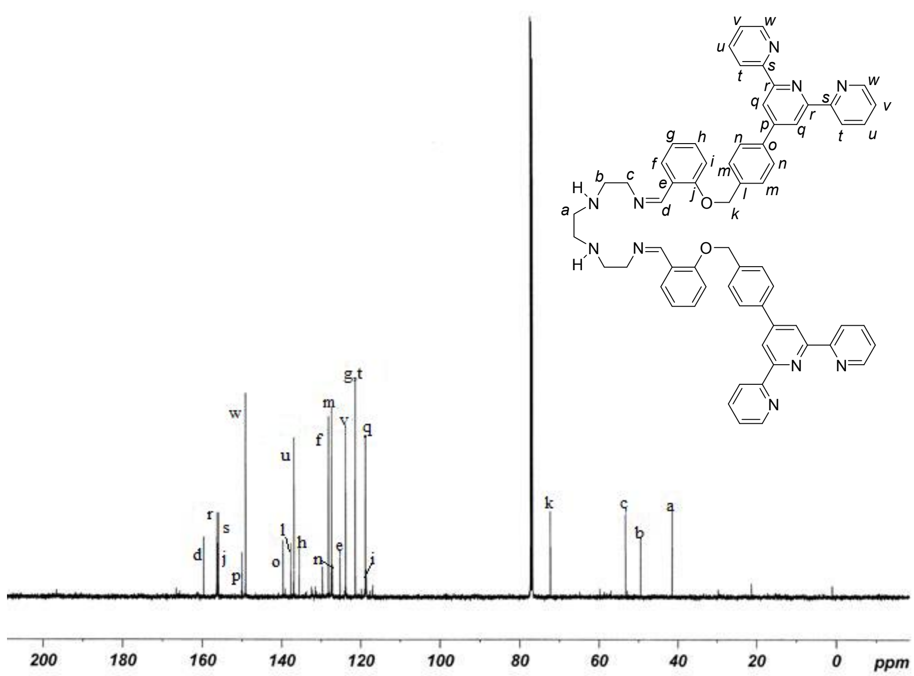

Figure S5. MALDI-TOF mass spectrum of $[Tb(NO_3)_2(\mathbf{L^2})](NO_3).5H_2O$ (**2**).

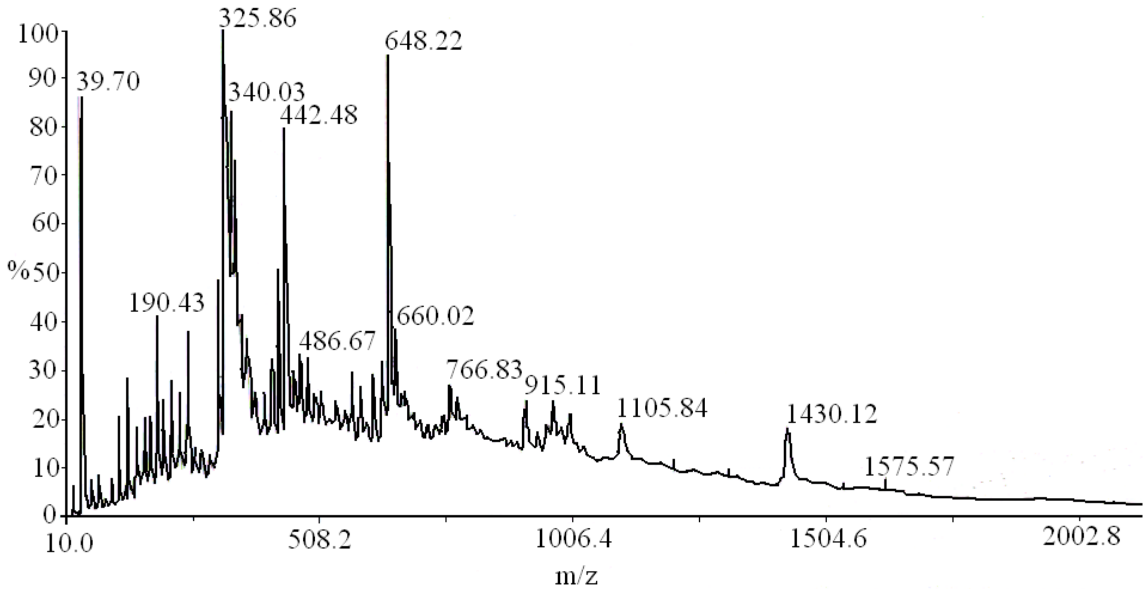

Figure S6. ESI mass spectrum of [Zn(ttpy)Cl_2] (**3**)

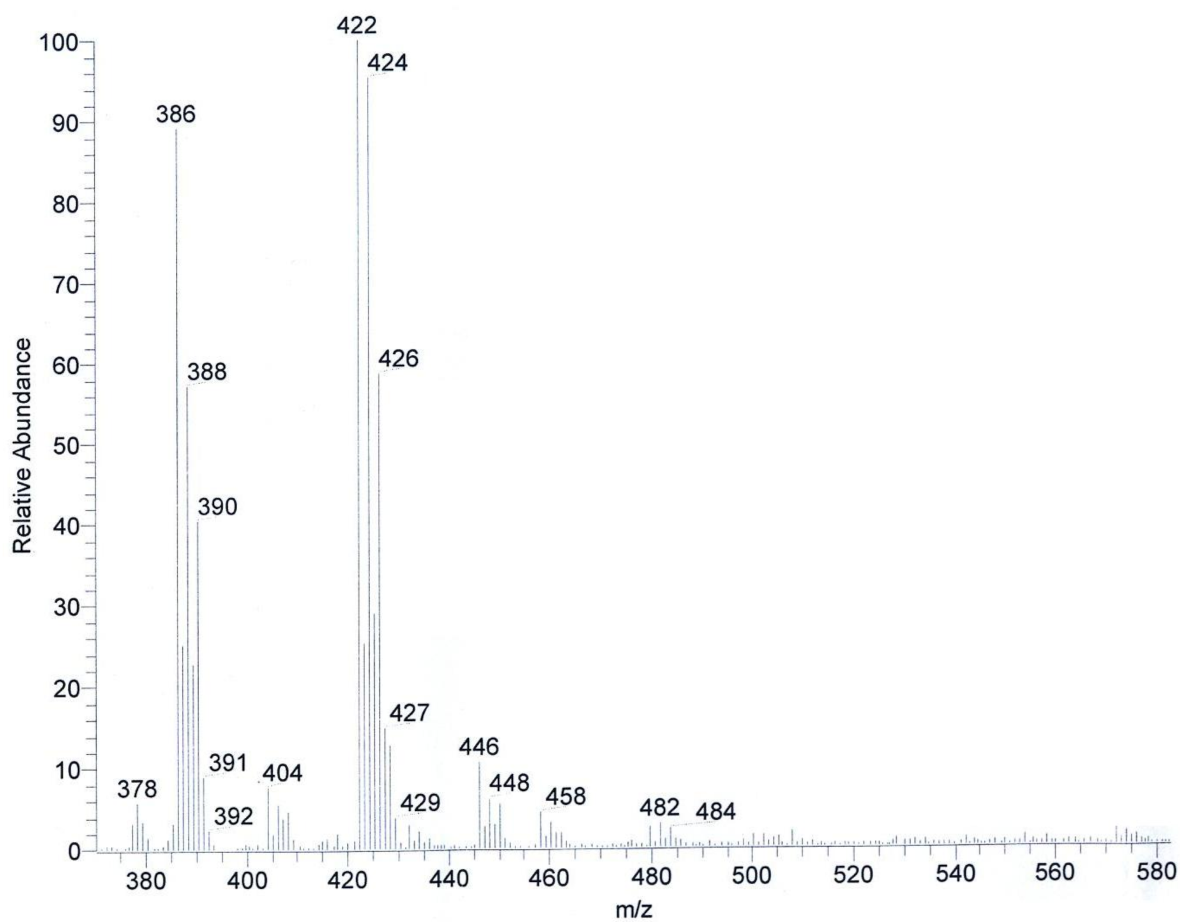

Figure S7. ESI mass spectrum of [Ru(ttpy)(**L**[1])]$(PF_6)_2$ (**4**).

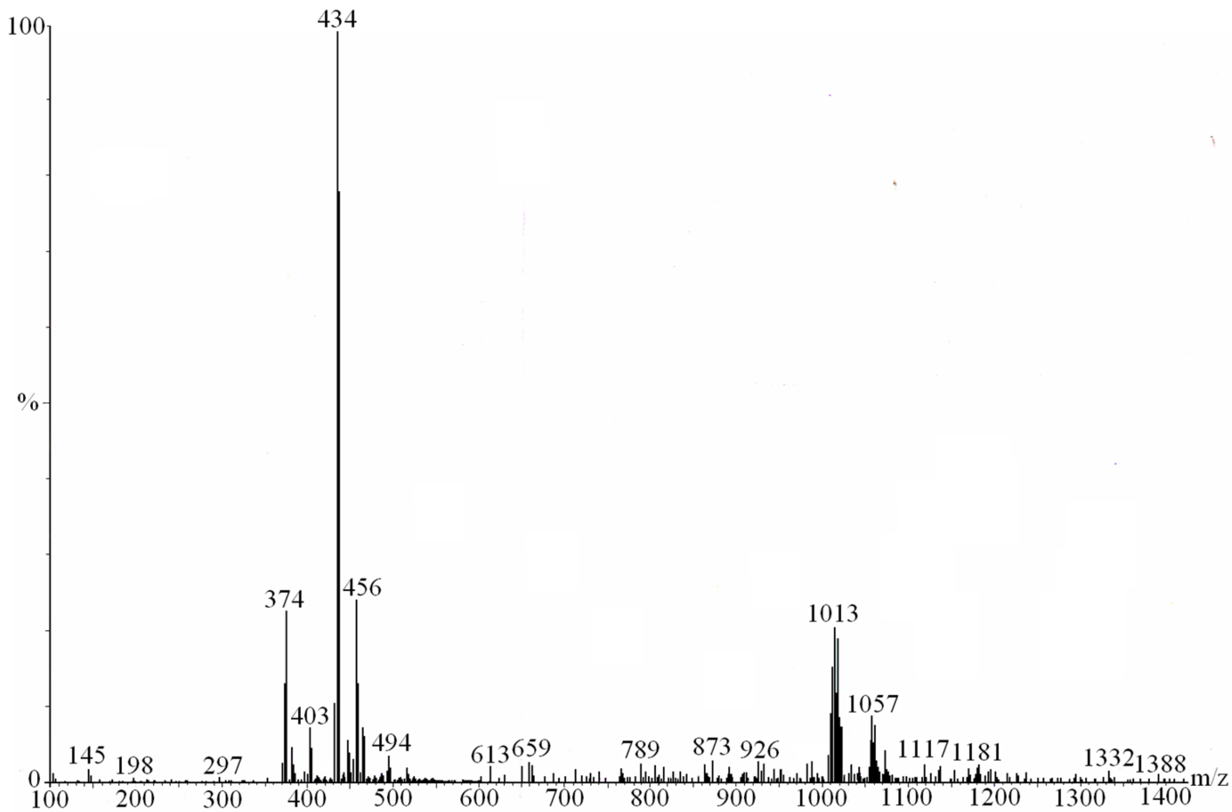

Figure S8. ESI mass spectrum of [{Ru(ttpy)}$_2$(**L**^{2})](PF_6)$_4$ (**5**).

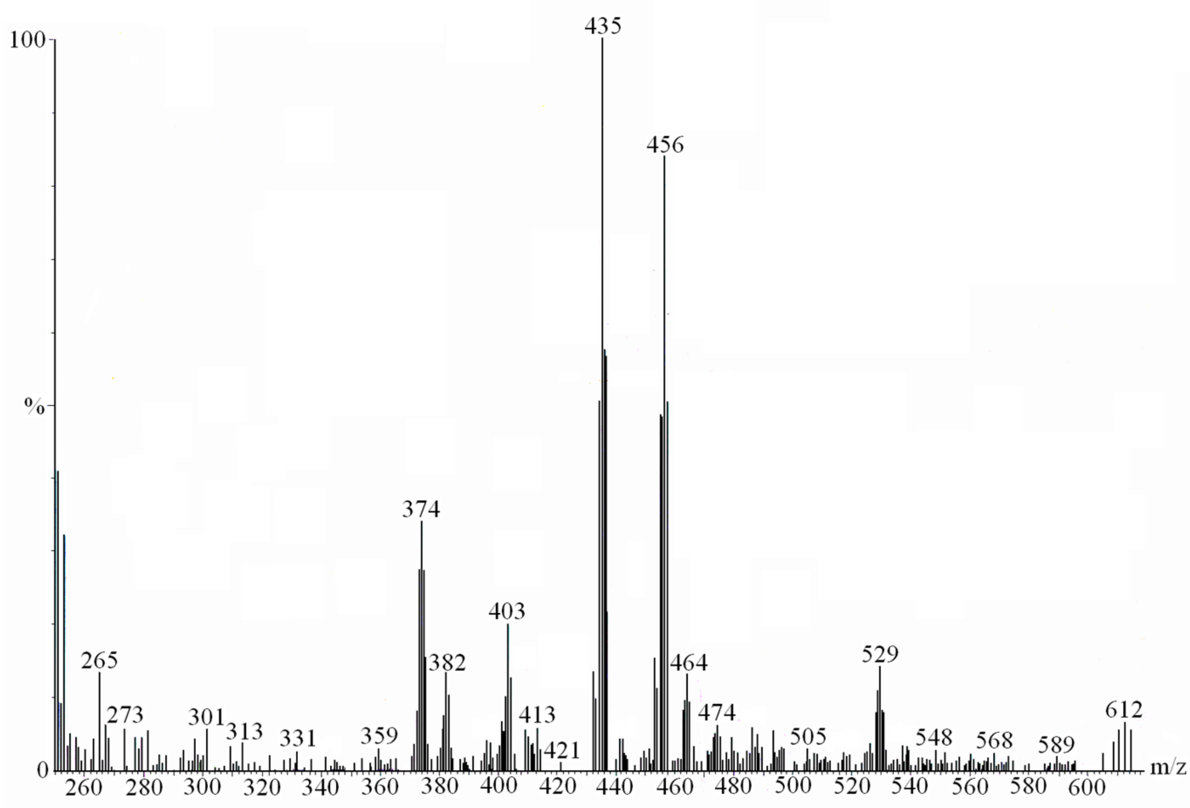

Figure S9. The ESI mass spectrum of $[Tb(NO_3)_2(\mathbf{L^2})\{Ru(ttpy)\}_2](PF_6)_5$ (**6**).

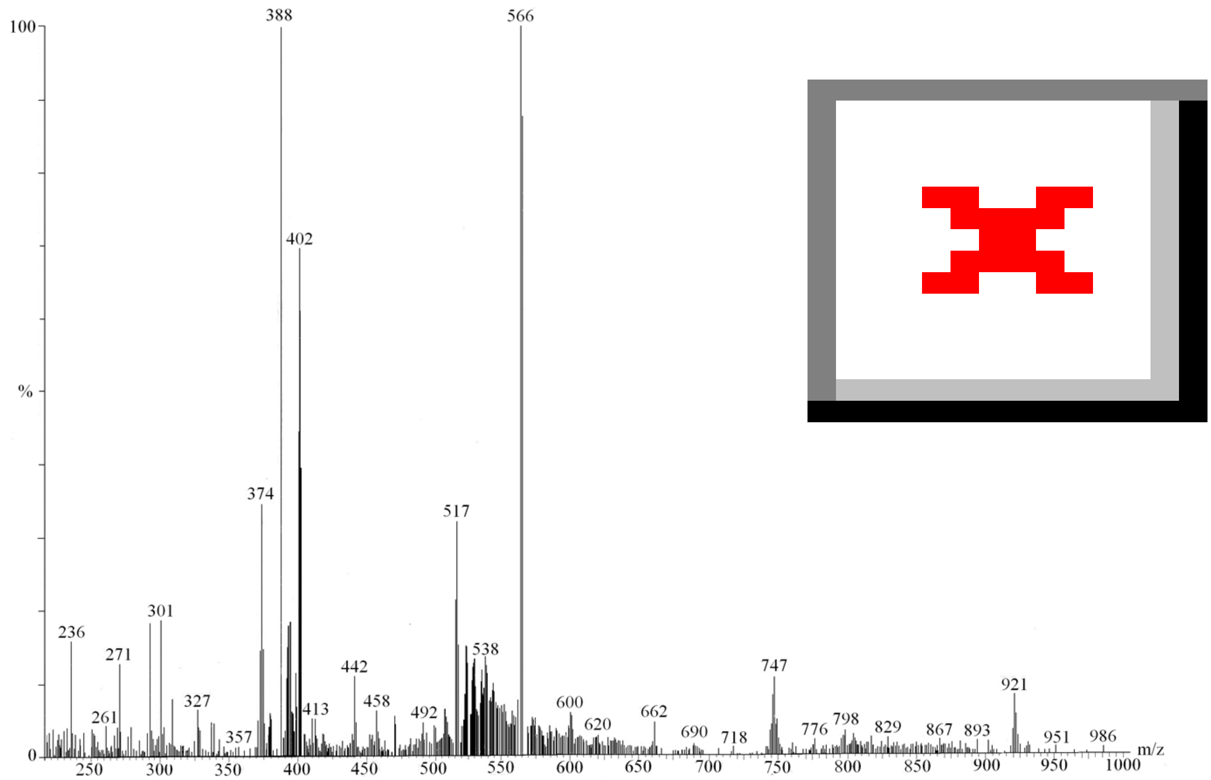

Figure S10. Electronic absorption spectrum of $\mathbf{L^2}$ in acetonitrile at 25 °C.

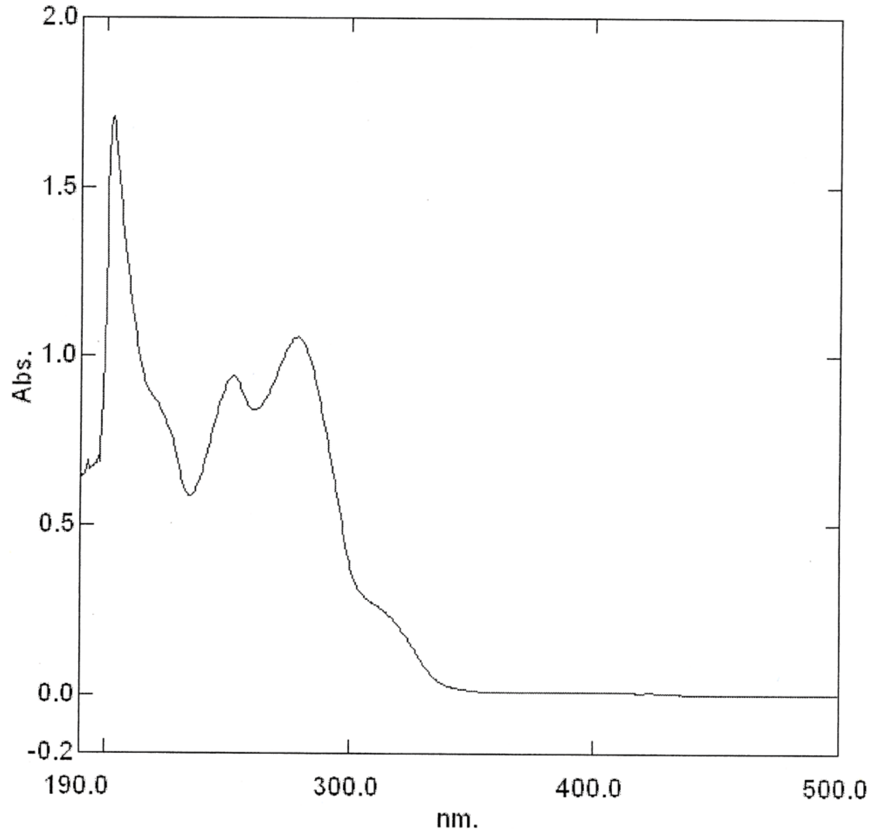

Figure S11. Emission spectrum of **L2** (λ_{ex} = 267 nm) in acetonitrile at 25 °C.

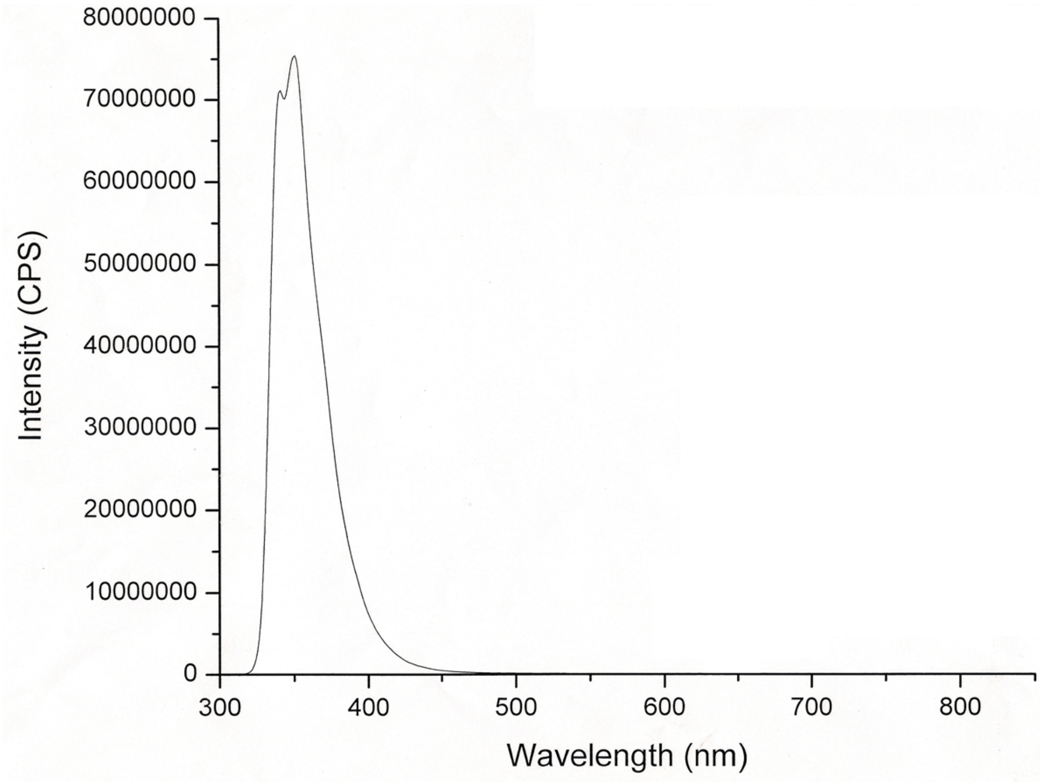

Figure S12. Electronic absorption spectrum of **2** in acetonitrile at 25 °C.

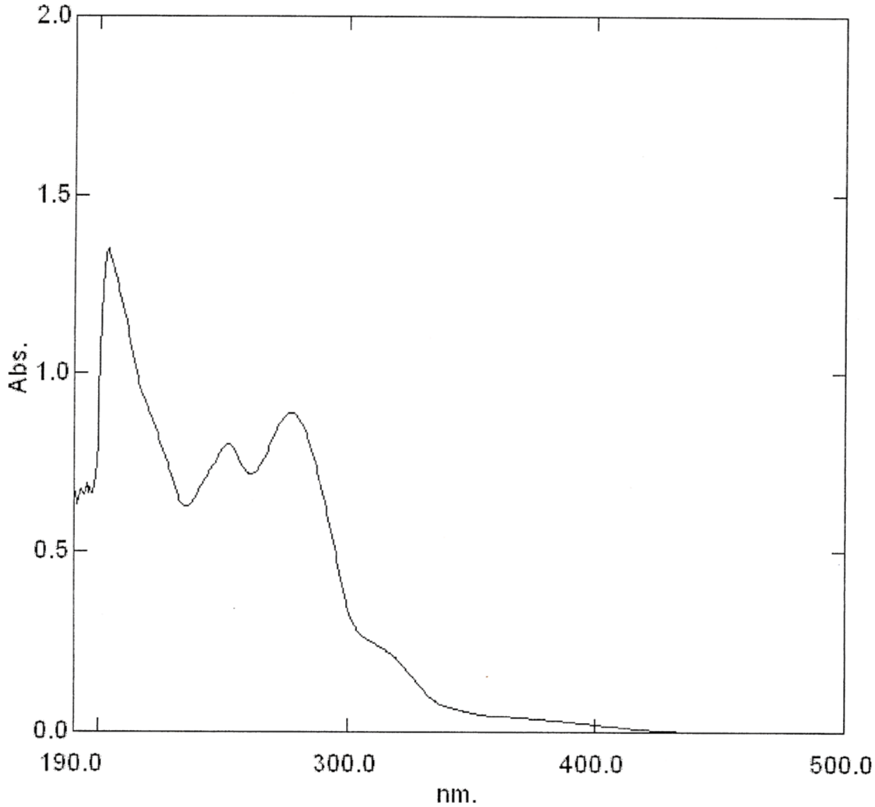
2.0
1.5
1.0
0.5
0.0
Abs.
190.0
300.0
400.0
500.0
nm.

Figure S13. Excitation spectrum of **2** (a) (λ_{em} = 545 nm), **5** (b) (λ_{em} = 698 nm), **6** (c) (λ_{em} = 687 nm) and **7** (d) (λ_{em} = 543 nm) in acetonitrile at 25 ºC.

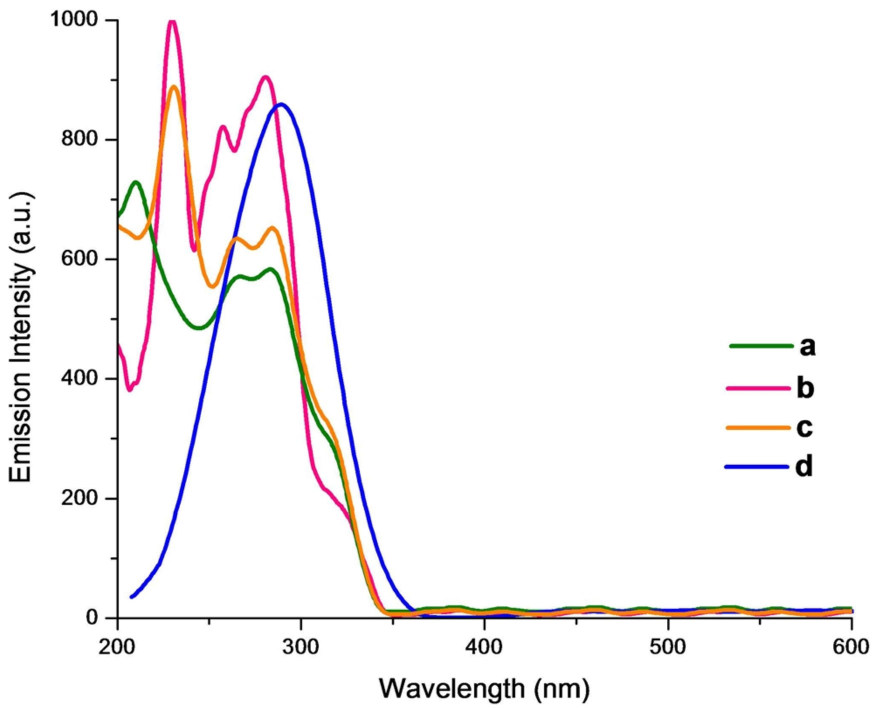

Figure S14. Electronic absorption spectrum of $[Tb(NO_3)_2(\mathbf{L^2})\{(Zn(ttpy)\}_2](NO_3)Cl_4$ (**7**) in acetonitrile.

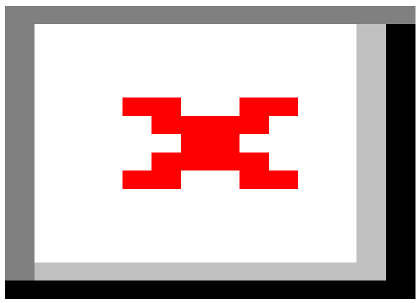

Figure S15. Emission spectrum of $[Tb(NO_3)_2(\mathbf{L^2})\{(Zn(ttpy)\}_2](NO_3)Cl_4$ (**7**) (λ_{ex} = 288 nm) in acetonitrile at 25 °C.

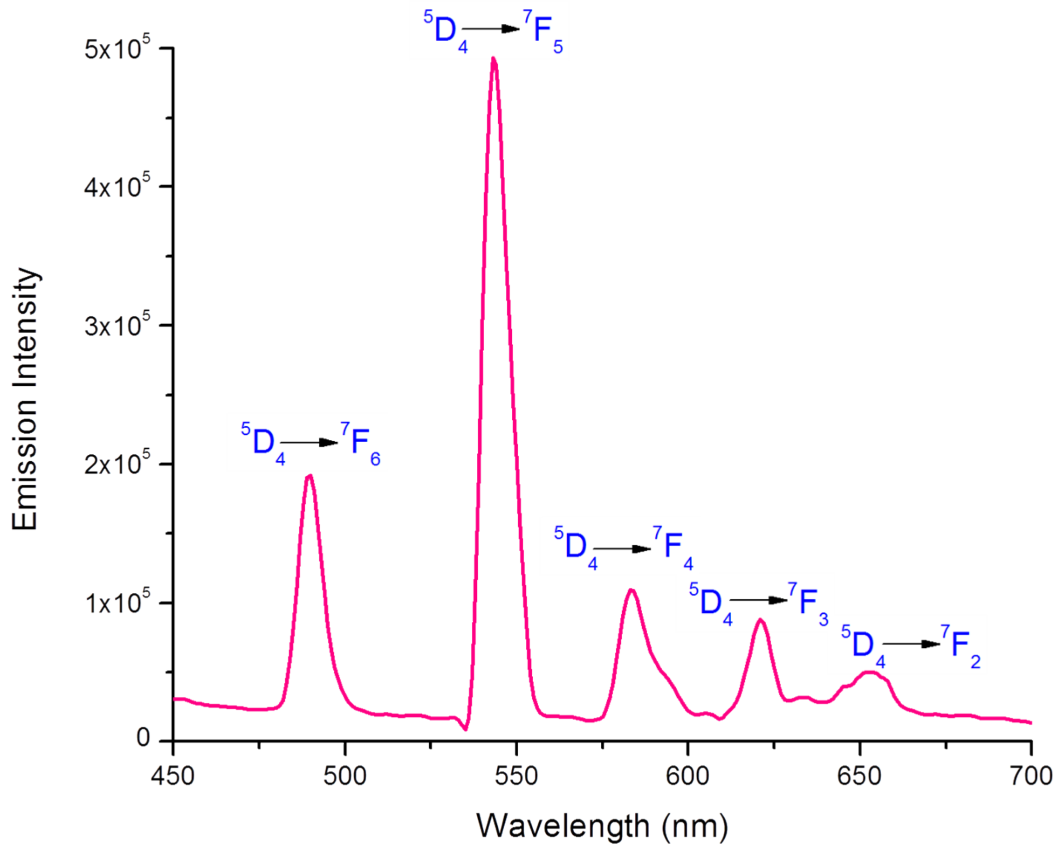

Figure S16. The cyclic voltammogram of [{Ru(ttpy)}$_2$(**L^2**)](PF_6)$_4$ (**5**) on a glassy carbon millielectrode in acetonitrile (0.1 M tetraethylammonium perchlorate) in the potential range 0 to 2 V versus Ag/AgCl at 25 °C, scan rate = 50 mV s^{-1}.

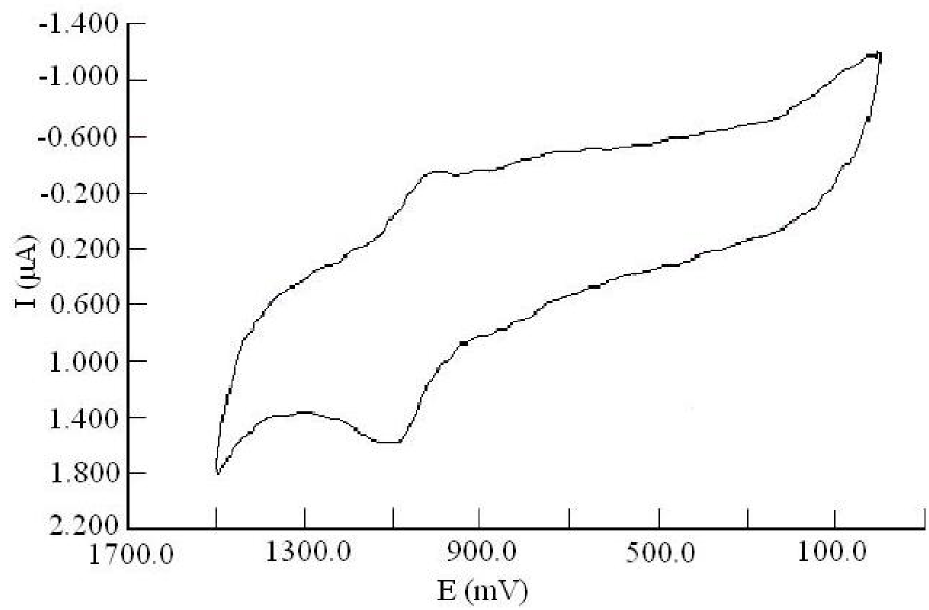

Figure S17. The cyclic voltammogram of [{Ru(ttpy)}$_2$(**L^2**)](PF_6)$_4$ (**5**) on a glassy carbon millielectrode in acetonitrile (0.1 M tetraethylammonium perchlorate) in the potential range 0 to –2 V versus Ag/AgCl at 25 °C, scan rate = 50 mV s^{-1}.

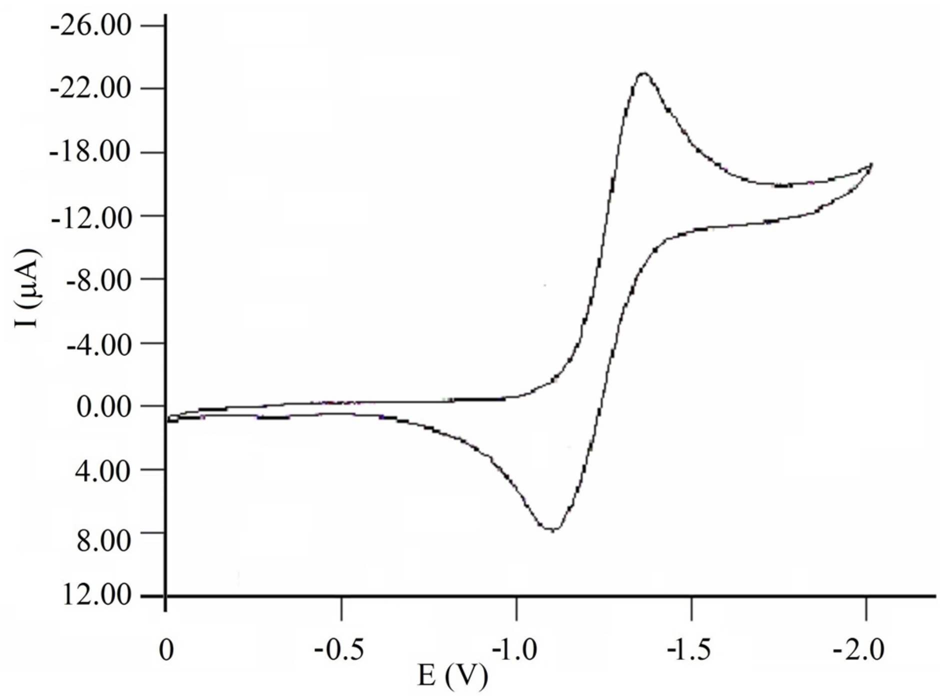

Figure S18. The cyclic voltammogram of $[Tb(NO_3)_2(\mathbf{L^2})\{Ru(ttpy)\}_2](PF_6)_5$ (**6**) in the potential range 0 to 1.2 V versus Ag/Ag^+ on a glassy carbon millielectrode in acetonitrile (0.1 M tetraethylammonium perchlorate) at 25 °C, scan rate = 50 mV s^{-1}.

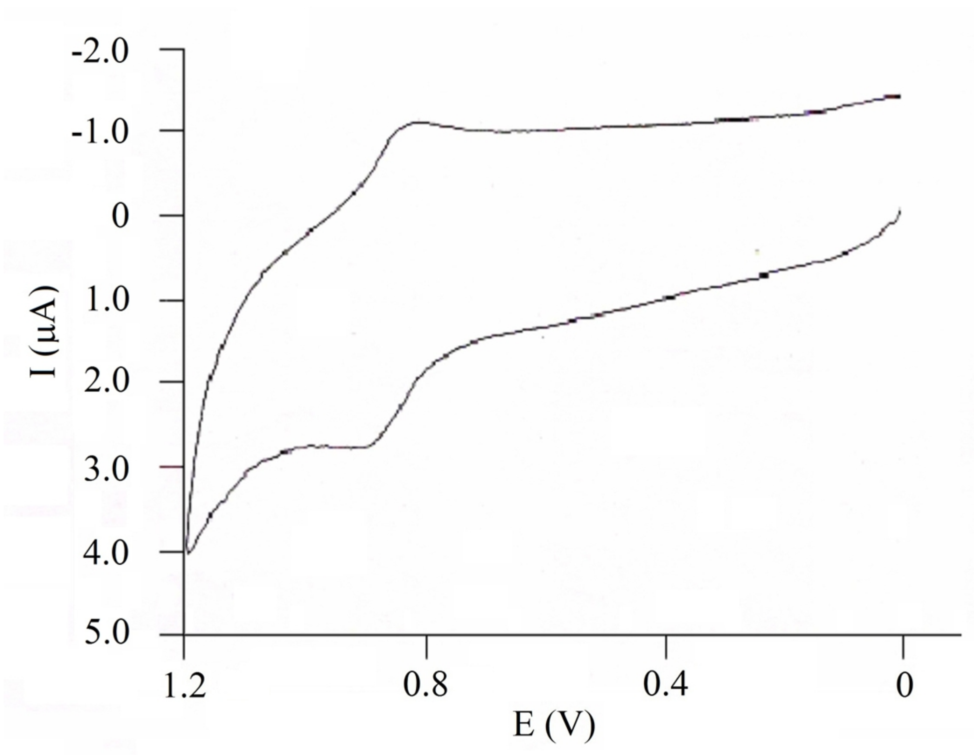

Figure S19. The cyclic voltammogram of $[Tb(NO_3)_2(\mathbf{L^2})\{Ru(ttpy)\}_2](PF_6)_5$ (**6**) in the potential range 0 to –2 V versus Ag/Ag^+ on a glassy carbon millielectrode in acetonitrile (0.1 M tetraethylammonium perchlorate) at 25 °C, scan rate = 50 mV s^{-1}.

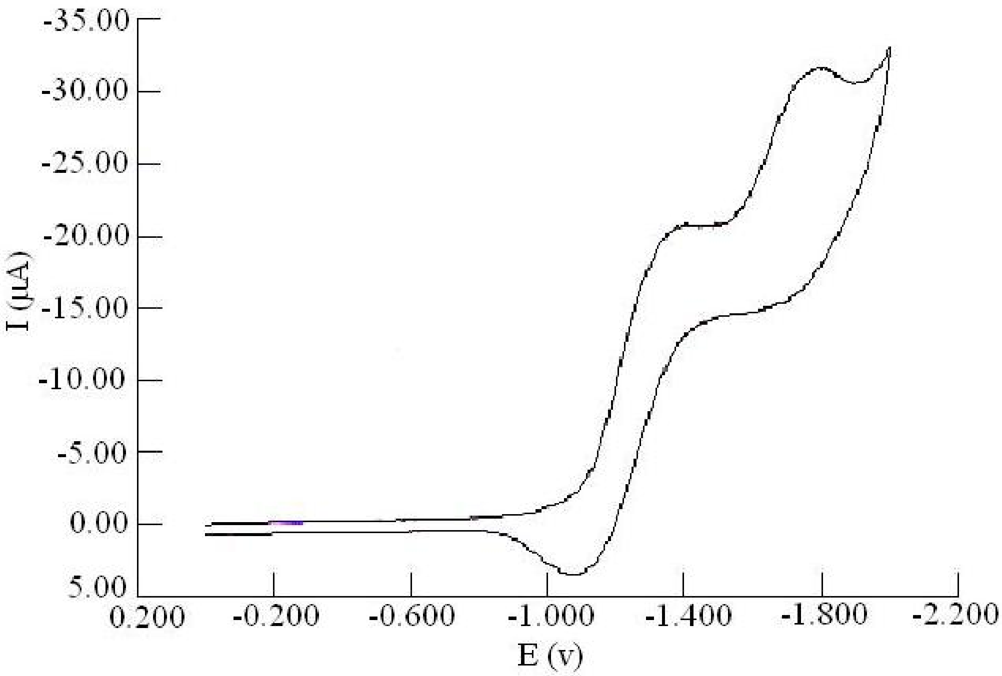

Figure S20. The cyclic voltammogram of $[Tb(NO_3)_2(\mathbf{L^2})\{Zn(ttpy)\}_2](NO_3)Cl_4$ (**7**) in the potential range -1 to -2 V versus Ag/Ag^+ on a glassy carbon millielectrode in acetonitrile (0.1 M tetraethylammonium perchlorate) at 25 °C, scan rate = 50 mV s^{-1}.